Available online at www.sciencedirect.com
ScienceDirect
Trans. Nonferrous Met. Soc. China 31(2021) 1303−1321
Transactions of Nonferrous Metals Society of China
www.tnmsc.cn

Processing and characterization of AZ91 magnesium alloys via a novel severe plastic deformation method: Hydrostatic cyclic extrusion compression (HCEC)

Armin SIAHSARANI, Ghader FARAJI

School of Mechanical Engineering, College of Engineering, University of Tehran, Tehran, 11155-4563, Iran

Received 10 June 2020; accepted 18 December 2020

Abstract: Capability of a novel severe plastic deformation (SPD) method of hydrostatic cyclic extrusion compression (HCEC) for processing of hcp metallic rods with high length to diameter ratios was investigated. The process was conducted in two consecutive cycles on the AZ91 magnesium alloy, and microstructural evolution, mechanical properties and corrosion behavior were investigated. The results showed that the HCEC process was successively capable of producing ultrafine-grained long magnesium rods. Its ability in improving strength and ductility simultaneously was also shown. The ultimate tensile strength and elongation to failure of the sample after the second cycle of the process were improved to be 2.46 and 3.8 times those of the as-cast specimen, respectively. Distribution of the microhardness after the second cycle was uniform and its average value was increased by 116%. The potentials derived from the polarization curves were high and the currents were much low for the processed samples. Also, the diameter of the capacitive arcs derived from the Nyquist curves was large in the HCEC processed samples. The finite element analysis indicated the independency of HCEC load from the length in comparison to the conventional CEC. HCEC is a unique SPD method, which can produce long ultrafine-grained rods with a combination of superior mechanical and corrosion properties.

Key words: severe plastic deformation; cyclic extrusion compression; corrosion behavior; mechanical properties; hydrostatic pressure

1 Introduction

Magnesium alloys are normally combinations of magnesium with other metals, such as aluminum, manganese, zinc, and copper, each of them provides a special property for the base metal. These alloys have a hexagonal close-packed (hcp) lattice structure with a c/a ratio of ~1.624. Furthermore, they have inadequate numbers of available slip systems at room temperature. Hence, their processing is more difficult and complicated than other metals with cubic lattice structure such as aluminum. The major application of the magnesium cast alloys is nowadays in automotive industry [1], and biomedical application [2]. However, their poor corrosion behaviors and lower mechanical properties limit their applications in industries, which need superior properties. AZ91 magnesium alloy is the most extensively used magnesium cast alloy and has a better combination of mechanical properties, corrosion resistance, and castability than others [3]. Grain refinement using severe plastic deformation techniques is one of the outstanding ways to achieve better properties in alloys [4,5]. It has been shown in most studies that performing severe plastic deformation processes such as equal channel angular pressing (ECAP) [6], cyclic extrusion compression (CEC) [7], high-pressure torsion (HPT) [8], and accumulative roll bonding

Corresponding author: Ghader FARAJI, Tel/Fax: +98-2161119966, E-mail: ghfaraji@ut.ac.ir
DOI: 10.1016/S1003-6326(21)65579-6

(ARB) [9], on different metals enhances the mechanical properties of the materials. However, about the effects of the severe plastic deformation methods on corrosion behavior, various trends have been reported. It has been reported that in the processes such as ECAP and rolling [10,11], which apply non-uniform strain to the sample, the corrosion resistance of the alloy decreases; but in the processes such as CEC [12], which applies more uniform strain or higher compressive force on the sample, the trend is vice versa.

On the other hand, there is a major drawback in severe plastic deformation methods, which is the limitation of all conventional SPD techniques in producing long samples due to the high amount of frictional forces between the die and the samples. This drawback limits their application in industrial scale. Therefore, efforts have been made in recent years to produce specimens with higher length to diameter ratios. SAMADPOUR et al [13] introduced a hydrostatic cyclic expansion extrusion (HCEE) method for the fabrication of long samples. They successfully produced a long sample of aluminum and magnesium alloys [5,13,14]. However, CEE based method has a limitation in applying uniform strain on the sample, which causes non-uniform microstructure and subsequently non-uniform properties. There are also other methods, which use hydrostatic pressure for processing and consequently producing long and large diameter samples such as hydrostatic radial forward tube extrusion [15] and hydrostatic extrusion [16], but the main characteristic of SPD method, which maintains the initial geometry of the sample was not considered in these processes.

Besides the ECAP and HPT methods, CEC is one of the primary processes of severe plastic deformation techniques. This process is one of the superior SPD methods and has lots of priorities than other SPD techniques. Unlike two other SPD methods, in the CEC more homogeneous strains can be introduced into the material due to the nature of the process. Besides, high strains in successive cycles of the process can be applied to the material without removing the workpiece from the die, which is not possible in ECAP. Also, due to the existence of high compressive stresses in this method, the formation of various materials and especially brittle metals is possible by applying high strains without cracks propagation [17].

The only limitation of the CEC process is its disability in producing the samples with a high length to diameter ratio due to the effects of frictional force and buckling of the processing punch in high ratios. So, the hydrostatic cyclic extrusion compression method can be introduced as one of the solutions for this disability [18]. In this process, the oil, which covers the workpiece, acts as the mean of applying high hydrostatic force to the sample. At the same time, it prevents direct contact of the workpiece and the die. The schematic of the process is illustrated in Fig. 1. At the first stage of the process, the sample is placed in the die and the oil is poured into the cavity between the die and the sample. The seal is inserted and the upper punch forces the sample to move through the deformation region. At this stage, the lower punch is fixed in its position. The material has reached this punch and forced to recover its initial diameter. After filling the gap, at the second stage, the whole material is processed by moving the punches and the sample in a downward direction. At this stage, the force of the upper punch is higher than that of the lower punch. For performing the second cycle of the process, the movement of the punches is reversed to the upward direction. At this stage, the force of the upper punch is smaller than that of the lower punch. So, a desirable number of the cycles and strain can be applied to the material by this procedure. The total strain after N passes of HCEC process (ε_N) is similar to the conventional CEC and is calculated from Eq. (1) [19]:

$$\varepsilon_N = 2n\ln\left(\frac{d_i^2}{d_e^2}\right) = 4n\ln\left(\frac{d_i}{d_e}\right) \quad (1)$$

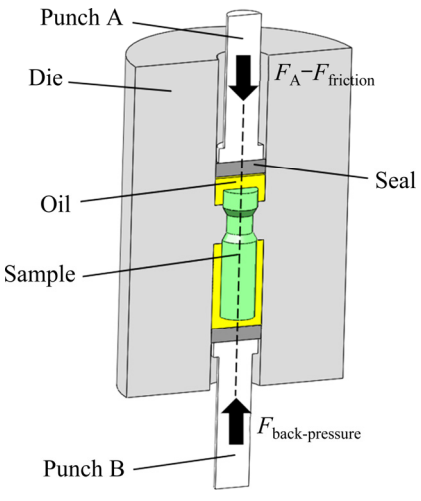

Fig. 1 Schematic representation of HCEC process

where d_i is the initial diameter of the rod and d_e is the diameter of the extrusion zone in the deformation region. By considering the die parameters used in this study, the theoretical total accumulated strain for each pass of the HCEC process is calculated as 1.15.

So, in this work, the hydrostatic cyclic extrusion compression was applied in two consecutive cycles on AZ91 magnesium alloys for producing long ultrafine-grained rods and microstructural evolution, mechanical properties and the corrosion behaviors of the samples were investigated and the results were compared with those of other studies. Finite element analysis was used for showing the effects of the increase in the length of the sample on the processing force. Furthermore, the variation of the strain distribution during the first and second cycles of HCEC and CEC was compared with each other by calculating the strain homogeneity index. Due to the lower amount of slip systems in magnesium alloys at room temperature, 300 °C is selected as the processing temperature. At higher temperature than 300 °C, the instability in the microstructure occurs in magnesium alloys, which causes the gradual grain coarsening [20].

2 Experimental

2.1 Material and HCEC process

AZ91 magnesium alloy with a chemical composition of 8.7% Al, 0.65% Zn, 0.25% Mn, and 0.014% Si, Fe, Be, Ni, and Cu was used as the processing material. The rods with an outer diameter of 12 mm and a length of 80 mm were prepared from the as-cast material. They were exposed to the one and two cycles of the HCEC process at 300 °C. The dies were fabricated from H13 steel and have the hardness of HRV 55. The samples with a diameter of 12 mm were extruded to the diameter of 9 mm and then expanded to their initial diameter. Furthermore, molten polyethylene was used as a pressurized fluid at 300 °C due to the evaporating of conventional oils at higher temperatures [21]. Pure copper was also selected as a sealant for the prevention of leakage in the contact areas [13]. The process was carried out at the ram speed of 5 mm/min.

2.2 Finite element simulation

A 2D analysis in the commercial Abaqus software was performed for simulation of the HCEC and conventional CEC processes and investigation of the variations in strain homogeneity and forces during the processes. To track the changes only in the samples, the dies and punches were considered as rigid parts and only the sample was considered to be deformable. The geometry of the sample was defined as the same as the experimental condition. Also, to show the effects of sample length on forming force during the HCEC and CEC, a sample with the double length of the experimental sample was simulated under the same conditions. The properties of the AZ91 magnesium at 300 °C were specified by conducting the tensile test and introduced to the software. The contact area between the sample and die surface in the HCEC was considered to be frictionless. In the deformation region, the friction coefficient at the interface was defined as 0.08. During the simulation of the conventional CEC process, the friction coefficients at all interfaces were considered as 0.08.

To evaluate the strain homogeneity in the specimens, they were tabulated and the strain homogeneity index (H) was calculated using Eq. (2) in the longitudinal cross-section of samples [22]:

$$H=\sum\left(\frac{\varepsilon_i}{\varepsilon_o}\frac{A_i}{A_o}\right) \tag{2}$$

where ε_i is indicative of the effective strain in each element, ε_o is the maximum effective strain in the studied area, A_i is the area affected by the effective strain and A_o is the total investigated area.

2.3 Microstructural evaluation

After performing the process, optical microscopy was used for investigation of the microstructure of the processed and unprocessed samples. The micrographs were captured from the perpendicular cross-section to the longitudinal direction of the samples after initial standard metallography preparation and etching for 15 s within a solution of 1% HNO_3, 24% $C_2H_6O_2$ and 75% water [23]. Furthermore, scanning electron microscopy (SEM) was used for further investigation of the cross-section of the processed rods.

2.4 Investigation of mechanical properties

Variation of the mechanical properties of the

samples was studied utilizing tensile and Vickers microhardness tests. The tensile test specimens were machined from the central region of the rod along the longitudinal direction according to ASTM E8 and the microhardness values were measured in the cross-section perpendicular to the longitudinal direction.

2.5 Corrosion behavior testing

Corrosion behavior was investigated using potentiodynamic polarization and electrochemical impedance spectroscopy (EIS) tests in 3.5 wt.% NaCl solution. NaCl is the most common solution in the investigation of the corrosion behavior of magnesium alloys and provides a good opportunity for comparison of the obtained results with other studies. The scans were carried out by three-electrode cells, the platinum as the counter electrode, Ag/AgCl as the reference electrode, and the sample with a surface of D=6 mm as the working electrode. The onset of the polarization scans was from the potential of −1.5 V OCP with a constant scanning voltage of 5 mV/s. Also, the obtained data were analyzed by Tafel fitting and the polarization resistance (R_p) was calculated by the derived data from the curve using Eq. (3):

$$R_p=\frac{\beta_a\beta_c}{2.3031J_{corr}(\beta_a+\beta_c)} \tag{3}$$

where β_c and β_a are indicatives of the slopes in the linear zones in cathodic and anodic regions of the Tafel area, and J_{corr} is the corrosion current density.

The frequency range for EIS measurements was from 10 mHz to 10 kHz, and the amplitude was selected to be 10 mV in proportion to the open-circuit potential. SEM micrography was used for tracking the variation of the surfaces for the unprocessed and processed sample after the corrosion test.

3 Results

3.1 Ultrafine-grained long magnesium rods

The HCEC process was carried out successfully in two consecutive cycles on the AZ91 magnesium rods at 300 °C. The unprocessed and two-cycle processed samples are shown in Fig. 2. As it is shown, in the deformation region the material was extruded to a lower diameter and then using the back-pressure by further processing the sample, it was returned to its initial diameter. It is worth mentioning that all these variations in dimensions and subsequently refining the samples are carried out by application of high hydrostatic pressure to the sample with the help of the pressurized hydraulic fluid, which is placed between the die and the specimen. Furthermore, this fluid eliminates the frictional force and makes it possible to refine and produce the samples with higher length to diameter (l/d) ratios than conventional SPD methods, which suffer from the higher frictional forces during the process [24,25].

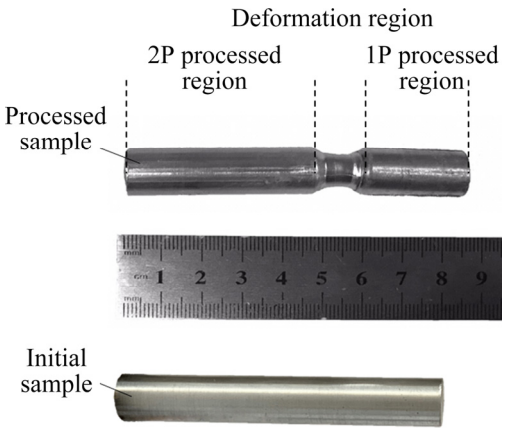

Fig. 2 Unprocessed and HCEC processed AZ91 magnesium samples after the second cycle

In Table 1 the length and diameter of the samples, which have been processed by the conventional CEC method and its derivative processes, are reported and compared with the HCEC process. As it is clear, the length to diameter ratio of the sample processed by HCEC in the present study is around 6.7. However, in the conventional CEC and CEE processes, the maximum reported ratios were around 2.8 and 4, respectively. This shows the capability of the HCEC process in producing the samples with a higher l/d ratio. Moreover, the HCEC process is able to refine even long samples due to the utilization of hydraulic fluid and subsequently prevention of the direct contact of the specimen and the die surface. This hydraulic fluid omits the limiting factor in conventional processes, which is high frictional forces and consequently reduces forming force and buckling of the forming punches. This issue was further shown and investigated by the FEM analysis.

Table 1 Length to diameter ratio of HCEE processed sample and its comparison with CEC and CEE processed samples

Process	Material	*l*/mm	*d*/mm	*l*/*d*	Source
HCEC	Mg−AZ91	80	12	6.7	This study
CEC	Al−4%Cu−Zr	24	10	2.4	[26]
CEC	Al−5%Mg	24	10	2.4	[27]
CEC	Al−SiC	50	30	1.7	[28]
CEC	Al	28	10	2.8	[29]
CEC	Al	8	8	1	[30]
CEC	Mg+nanotubes	42	30	1.4	[31]
CEC	Mg−1.5%Zn−0.25%Gd	42.5	39	1.09	[32]
CEC	GW102K-Mg alloy	42	29.5	1.4	[33]
CEE	AM60 Mg alloy	40	10	4	[34]

3.2 Finite element results

Figure 3(a) illustrates the variation of the processing force against ram movement obtained from FEM analysis for the CEC and HCEC processing of AZ91 magnesium rods at 300 °C, and the maximum required force for each state is depicted in the histogram of Fig. 3(b). In order to show the major achievement of the HCEC process, which is the independency of the HCEC from the length of the processing sample, a longer rod with a length of 16 cm (2 times greater than the experimental sample) with the same diameter was simulated and the processing force was compared. As it is clear from the results, the maximum forming force during the HCEC processing of the magnesium sample with a length of 8 cm is around 49.7 kN. However, this force increases to 99 kN in CEC processing of the sample with the same length. On the other hand, CEC processing of the magnesium sample with a length of 16 cm requires the maximum force of 320 kN, which is 3.2 times that of the CEC processing of the magnesium sample with the length of 8 cm at 300 °C. However, as it is clear the trend in increasing the processing force during the HCEC process and the maximum required force for processing of the sample with a length of 16 cm is almost the same as the sample with a length of 8 cm. This issue further illustrates one of the major characteristics of the HCEC process, which is its capability in producing the samples with the desired *l*/*d* ratio without a restriction in increasing the processing force, unlike the conventional CEC. The same results were achieved in the processing of the AM60 magnesium rods by the hydrostatic cyclic expansion extrusion (HCEE) [35].

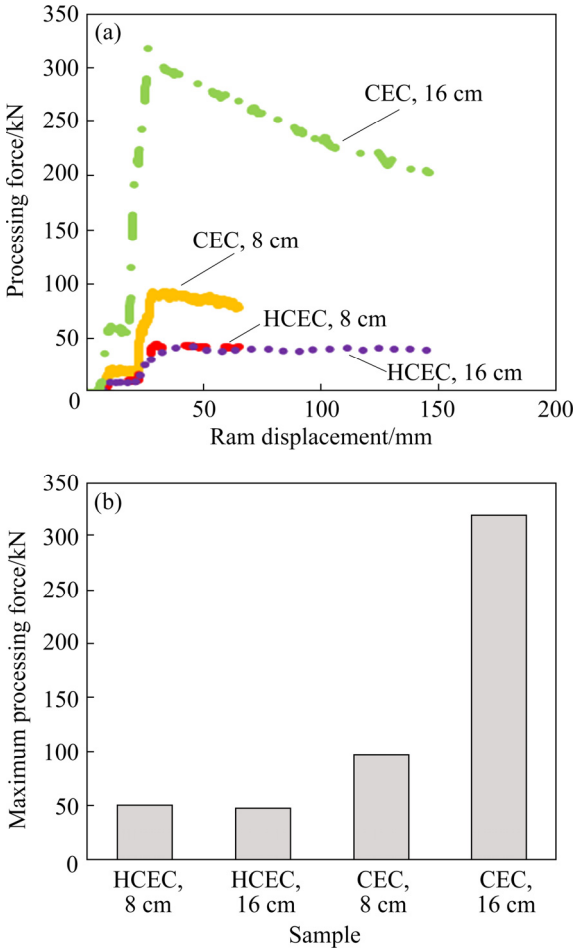

Fig. 3 Variation of processing force derived from FEM (a) and maximum processing force for CEC and HCEC processing of AZ91 magnesium alloy rods with different lengths at 300 °C (b)

The color-coded contours of the strain distribution after the first and second cycles of the HCEC process on AZ91 magnesium rod is shown in Fig. 4(a). For comparison of the results, the conventional CEC process was also simulated in the same condition and the results for strain distribution after the first and second cycles are also shown. As it is illustrated, the strain distribution along the longitudinal direction of the HCEC processed rod is homogenous. However, in the radial direction, the distribution is different and the variation is seen. The contours of the CEC processing of magnesium rods show more inhomogeneity rather than the HCEC process and especially after the second cycle

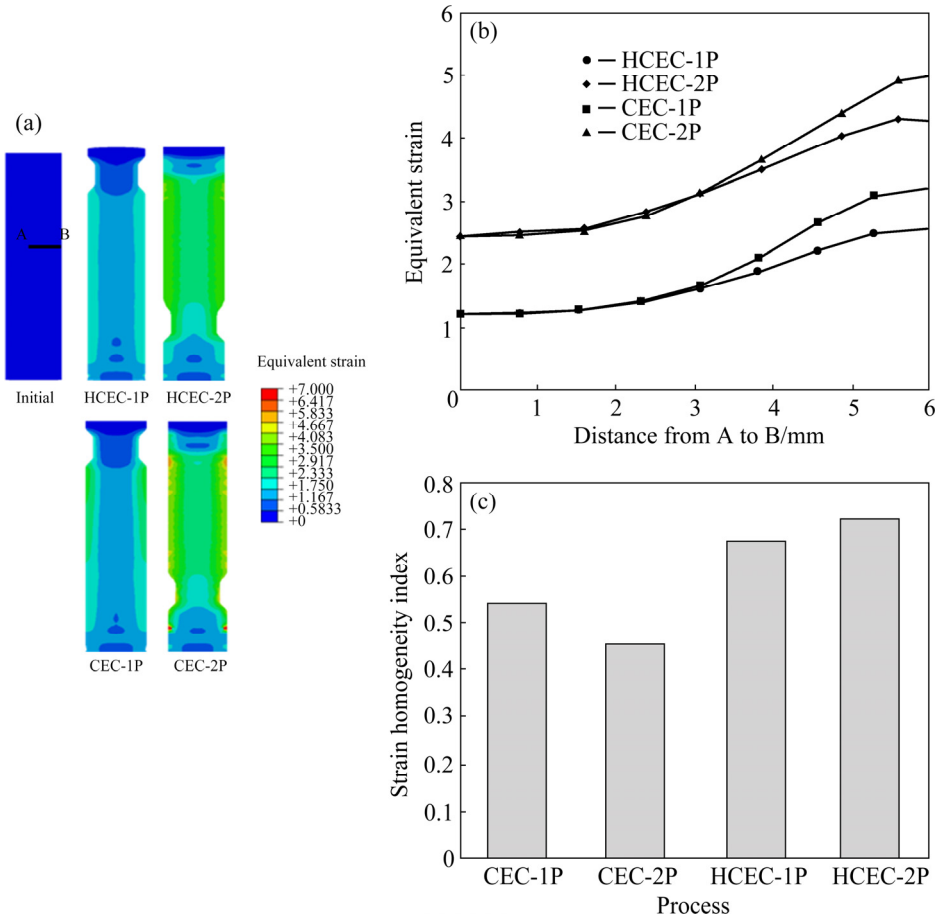

Fig. 4 Color-coded contours of strain distribution after the first and second passes of HCEC and CEC for AZ91 magnesium rods (a), curves of strain along path from A to B (b), and strain homogeneity index in longitudinal direction for one and two passes processed rods after HCEC and conventional CEC (c)

of the CEC. To better show the inhomogeneity of strain in the radial direction, the strains along the path from A to B (Fig. 4(a)) after the first and second cycles of both CEC and HCEC are shown in Fig. 4(b). As it is clear, the homogeneity along this path after the HCEC is better than the CEC process in the both first and second cycles. In the inner regions, the strains in both processes are the same, but in outer regions, the strains in the CEC process are larger, which causes further inhomogeneity in strain and subsequently variation in different properties of the processed rods. Furthermore, by comparison of the strain homogeneity between the first and second cycles in both processes, more inhomogeneity in the second cycles is shown in the radial direction. The overall homogeneity of the sample was analyzed by calculating the strain homogeneity index and the results are shown in Fig. 4(c). For this measurement, the strain values over more than 500 elements were specified and the index was calculated using the Eq. (2). This diagram further confirms the fact that there is more inhomogeneity in the CEC process than the HCEC. The homogeneity indexes after the first cycle of the CEC and HCEC are 0.54 and 0.67, respectively. In the CEC process, the inhomogeneity after the second cycle increases and the index decreases to 0.45. However, in the HCEC process, the trend is vice versa. Although the homogeneity after the second cycle of HCEC in the radial direction decreases, the overall homogeneity after the second cycle of the HCEC process is more than the first cycle. The homogeneity index after the second cycle of HCEC is 0.71. This leads to other outstanding characteristics of the HCEC process, which is its capability in the insertion of more homogenous strain to the sample rather than the conventional CEC.

For confirmation of the accuracy of the FEM analysis, the experimental and FEM obtained forces during the first pass of the HCEC process by processing the magnesium rods were compared and

the highest difference of about 9% was seen.

3.3 Microstructure

Optical micrographs of AZ91 magnesium rods for the initial state and the HCEC processed ones after the first and second cycles of the process are illustrated in Fig. 5. Furthermore, SEM images showing the microstructure in higher magnification for the samples after the HCEC process are shown in Fig. 6. The microstructure of the initial as-cast AZ91 magnesium is depicted in Fig. 5(a). The same microstructure as other studies with a primary magnesium α-phase, net-like eutectic α-phase, and β-phase is distinguishable in the micrograph [10,36]. As it is clear, the β-phase is embedded in the primary and eutectic magnesium phases. The β-phase has more amount of Al in comparison to the α-phase and it is irregular release of $Mg_{14}Al_{12}$.

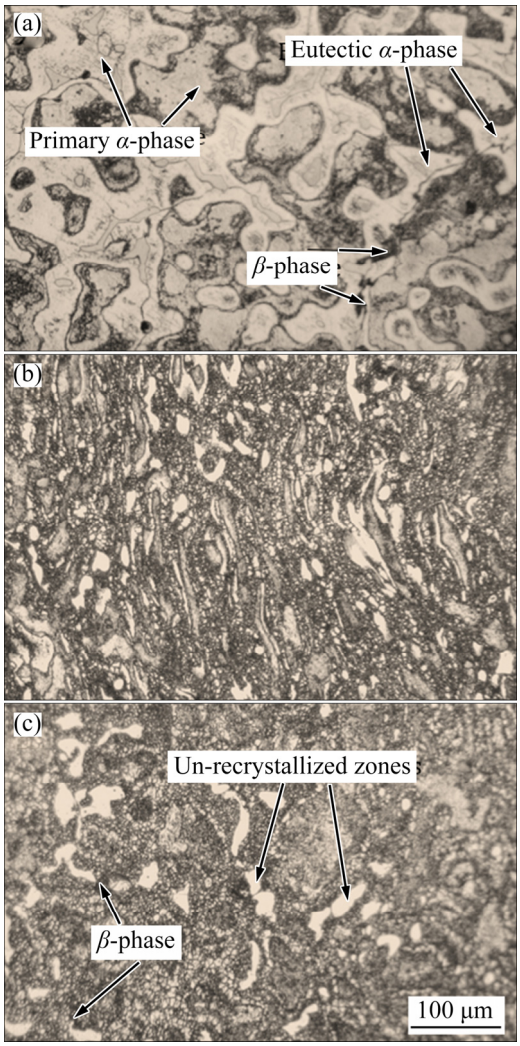

Fig. 5 Optical micrographs of AZ91 magnesium for initial (a), one-pass (b), and two-pass (c) HCEC processed samples

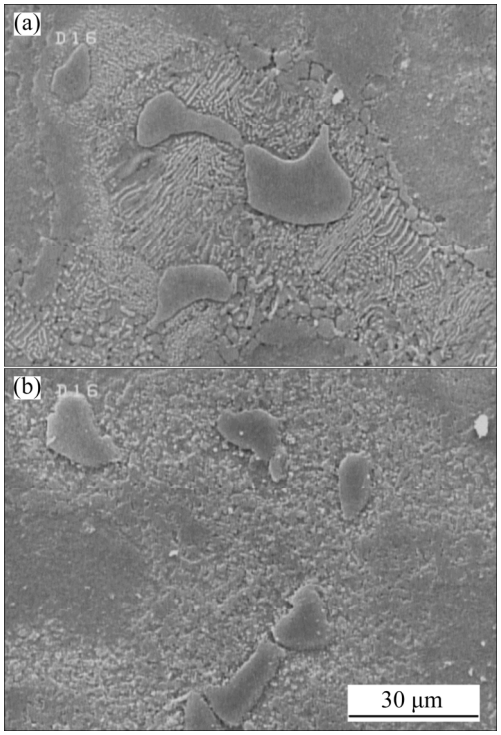

Fig. 6 SEM images of HCEC processed magnesium rods after the first (a) and second (b) cycles

By performing the process and subsequently imposing severe strain, the ultrafine microstructure is created after the first and second passes of the process and the structure is different from the initial state. The microstructure after both cycles is relatively inhomogeneous and the size of the most formed grains is in the range of 1−3 μm. However, some coarse grains with a size of more than 10 μm also exist. Furthermore, some nanograins especially after the second cycle are formed, which are difficult to observe in optical images. As it is shown in Fig. 5(b), after the first cycle the main reduction in grain size occurred and the imposed shear strain during the process has caused the phases to distort and elongate in the flow direction of the material. Moreover, the eutectic structure and also the second phase were broken into small parts. Generally, an elongated structure of fine α and β phases is seen beside the uncrystallized zones and coarse β phases, which has been previously reported in the SPD processing of AZ91 alloys at a higher temperature and moderate strain range [37]. As shown in Fig. 5(c), after processing the AZ91 sample at the second cycle of the HCEC, the amount of the elongated grains decreases and a fine-grained equiaxed microstructure is formed. An almost

isolated and mostly fine microstructure is seen. Furthermore, the amount of the unrecrystallized regions decreases and more $Mg_{17}Al_{12}$ particles become smaller. However, some undissolved $Mg_{17}Al_{12}$ particles are still detectable in the microstructure. Like other SPD techniques, the major reduction in grain size is more evident at the initial stage of the process and not notable at higher strain levels in the second pass [25]. By analyzing the SEM images in Fig. 6 for the processed samples after the HCEC process, decreasing the size of the grains, breaking the β phase particles and their uniform distribution are seen. The elongations of the grains and particles and lamellar distribution of the fine β phase after the first cycle and their more homogenous distribution after the second cycle are also evident [10]. The images show the potential of the HCEC process in grain refinement of the magnesium alloys and its more homogenous distribution of grains and particles rather than other SPD techniques like ECAP [38].

3.4 Mechanical properties

The engineering stress−strain curves of the AZ91 magnesium alloy before and after the HCEC process are depicted in Fig. 7(a). An outstanding increase in the strength and ductility of the magnesium sample was achieved after the HCEC process. The initial sample had the ultimate strength and elongation of 158.1 MPa and 3.6%, respectively. By performing the first cycle, the ultimate strength and elongation increased respectively to 307.2 MPa and 8.2%, respectively, which are 1.94 and 2.27 times those of the initial sample. The highest strength and elongation were obtained after the second cycle. The strength and elongations are 390.5 MPa and 13.7%, respectively. The major increase in the ultimate strength occurred after the first and second cycles, the increase rate in strength is lower. However, the increased rate in elongation after the second cycle is more. This combination of high strength and elongation after the HCEC process shows considerable potential in producing ultrafine-grained rods with superior mechanical properties. Furthermore, this feature is combined with its notable capability in producing the sample with high length to diameter ratios, which makes the HCEC process unique method between different SPD techniques for industrial application.

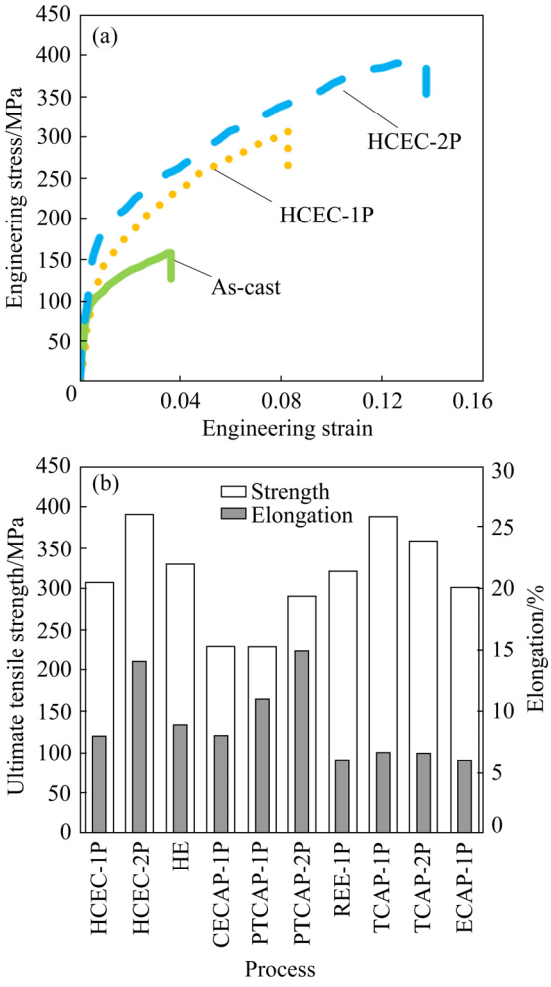

Fig. 7 Engineering stress−strain curves for initial and HCEC processed AZ91 magnesium samples (a) and elongation and ultimate strength after HCEC process and its comparison with other techniques (b)

Figure 7(b) illustrates the ultimate tensile strength and elongation after the first and second cycles of the HCEC process and its comparison with other processing techniques such as hot extrusion (HE) [39], extrusion compression angular pressing (CECAP) [40], parallel tubular channel angular pressing (PTCAP) [41], tubular channel angular pressing (TCAP) [37] and equal channel angular pressing (ECAP) [42], which were performed on AZ91 magnesium alloys at higher temperatures of 200 and 300 °C. The results indicate the achievement of higher ultimate strength after the second cycle of the HCEC process in comparison to other processing methods. By comparison of the ultimate strength after the first cycle of HCEC, it can be seen that performing the first cycle of the HCEC provides higher strength than one pass of the CECAP, PTCAP, RFE and

ECAP processes. However, the strength is lower than the one-pass processed sample by TCAP at 200 °C. Also, that of the strength after the first cycle is higher than that of two-pass processed sample by PTCAP method. Moreover, higher elongation after the HCEC process was achieved in comparison to the HE, CECAP, RFE, TCAP and ECAP processes. But the obtained elongation after the second cycle is lower than two-pass processed sample by PTCAP. The ultimate strength after the second cycle of HCEC is almost the same as the one-pass processed tube by TCAP. However, the elongation results indicate much difference between them and for the two-pass processed HCEC rod, it is much higher than the tube processed by TCAP. The higher mechanical properties in PTCAP and TCAP processes along with HCEC are caused by higher hydrostatic pressure in the processes. However, better combination of the strength and elongation is more notable for the HCEC processed magnesium comparing with the TCAP and PTCAP processes.

The number fraction of microhardness values, which shows the percentage of them in each range, for the AZ91 magnesium rods before and after the HCEC process is depicted in Fig. 8. The histograms show a reduction in the width of the microhardness distribution by performing the HCEC in the second pass rather than the first pass processed sample and the initial state. The microhardness variation in the initial sample is in the range of HV 46−64. However, the most fraction is between HV 46−54 and higher values have a lower percentage. After the first cycle of the HCEC process on magnesium rod, the vales of microhardness reached HV 94−110. By conducting the second cycle the microhardness range changed to HV 104−116. This indicates the improvement in distributing the hardness by an increase in the number of the HCEC passes. Furthermore, the average microhardness shows a similar trend like ultimate tensile strength and increased to the average value of HV 99.1 after the first cycle of HCEC in comparison to the initial value of HV 49.8. After the second cycle, the hardness reached HV 107.6. The changes of the microhardness are completely in agreement with the variation of the tensile properties and further confirm the capability of the HCEC process in improving the mechanical properties of the magnesium alloys.

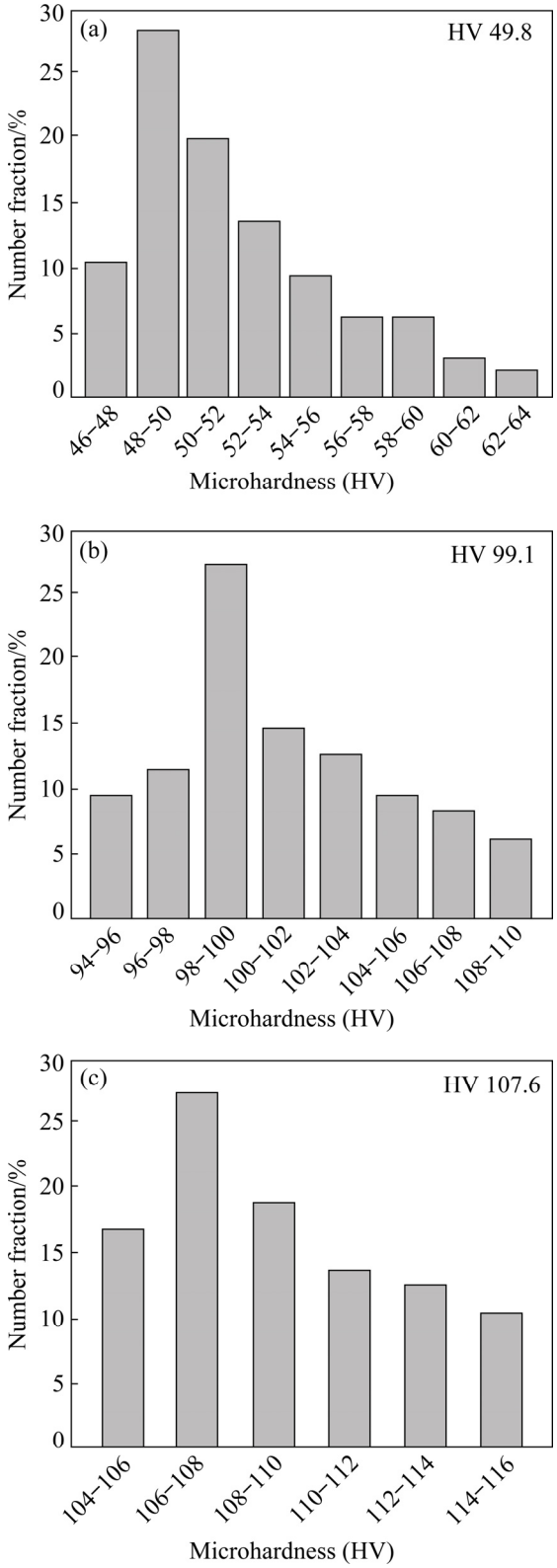

Fig. 8 Histograms of hardness distribution in cross-section of initial (a), one-cycle (b), and two-cycle (c) HCEC processed AZ91 magnesium alloys

The average values of the Vickers microhardness after the first and second cycles of the HCEC process are compared in Table 2 with

the other SPD techniques such as RFE [43], PTCAP [44], CECAP[40], and TCAP [37]. The overall trend in the achieved microhardness is in agreement with other techniques. By comparing with other SPD methods, the HCEC process is a unique technique that provides higher microhardness for the AZ91 magnesium alloy. The average microhardness after the first cycle of the HCEC process is more than RFE, CECAP, and is almost the same as the processed AZ91 magnesium sample after three passes of PTCAP and two passes of TCAP. After the second cycle of HCEC, the microhardness is much higher than other presented methods.

Table 2 Comparison of Vickers microhardness results for AZ91 magnesium samples after HCEC method with other SPD techniques

Process	Microhardness (HV)	Source
HCEC-1P	99.1	This study
HCEC-2P	107.6	This study
RFE-1P	87	[43]
PTCAP-1P	75	[44]
PTCAP-2P	95	[44]
PTCAP-3P	99	[44]
CECAP-1P	90	[40]
TCAP-1P	93	[37]
TCAP-2P	99	[37]

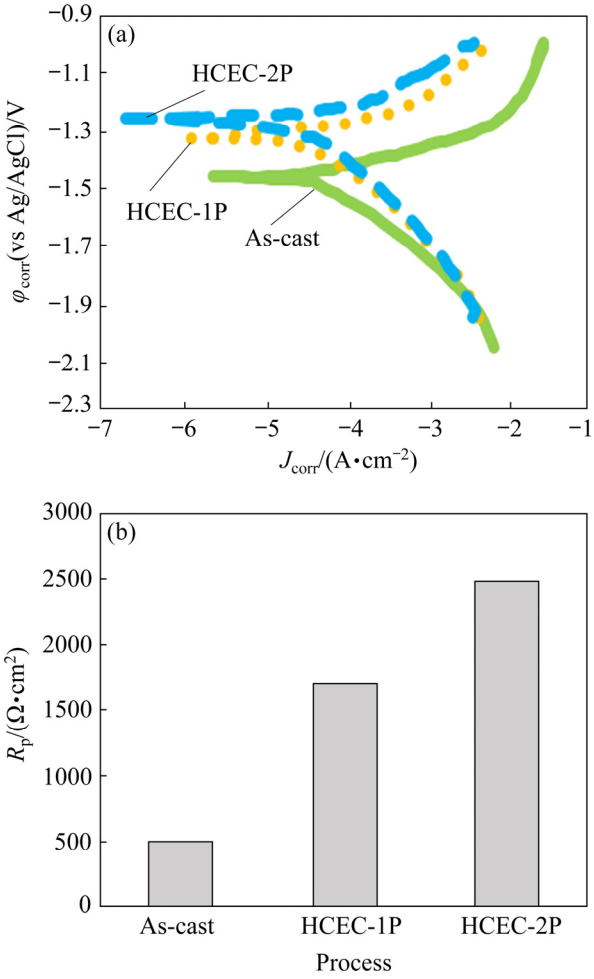

Fig. 9 Polarization curves (a) and calculated polarization resistance from polarization curve (b) for unprocessed and HCEE processed AZ91 magnesium alloy

3.5 Corrosion behavior

Figure 9(a) shows potentiodynamic polarization curves for the as-cast AZ91 magnesium rod and HCEC processed samples after the first and second cycles. Furthermore, the values of the polarization resistance (R_p) for the samples after deriving the corrosion parameters by Tafel fitting such as potential (φ_{corr}), J_{corr}, β_c and β_a coefficients were calculated using Eq. (3) and the values are presented in Fig. 9(b). The J_{corr} values were determined by extrapolating the linear anodic and cathodic regions in the curves. As shown in Fig. 9(a), all the samples indicate analogous polarization diagrams. This presents the resembling corrosion manner for the initial and processed samples. The processed sample after the first cycle of the HCEC shows higher potential than the unprocessed one, which indicates its higher electrochemical corrosion characteristic at the beginning of the corrosion. Furthermore, the HCEC processed sample shows a lower corrosion current density in comparison to the initial state. Moreover, performing the second cycle of the HCEC process has led to an increase in potential and a further decrease in the current density. The results represent the capability of the HCEC process in improving the corrosion properties of the magnesium rods in an aqueous solution of 3.5 wt.% NaCl. This is further shown in the comparison of the R_p values in Fig. 9(b). As it is shown, the HCEC processed sample after the first and second cycles showed 3.5 and 5 times polarization resistance of the initial sample, respectively. Higher anodic kinetics and lower cathodic kinetics and subsequently higher current density in the unprocessed sample play an important role in lower resistance. The derived values of the φ_{corr} and J_{corr} for the one- and two-

cycle processed AZ91 magnesium from the polarization curves were compared with obtained results for pure magnesium and AZ91 alloy after different processes such as ECAP [10,45], HPT [11], and hot rolling followed by ECAP [11] in Table 3. Furthermore, the results for the initial sample of each state are depicted in Table 3. It is clear that HCEC process provides a higher φ_{corr} and a lower J_{corr} for the AZ91 magnesium alloy in comparison to other SPD techniques such as ECAP. The obtained results are near to the results of pure magnesium after the HPT process. It has been shown that AZ91 alloy indicates worse corrosion properties than pure magnesium [46]. This issue is also shown in Table 3 by comparison of the results prior to processing for the pure Mg and AZ91 magnesium alloy. The AZ91 alloy investigated in the present study had the current density of around 47 μA/cm^2. However, the pure magnesium showed the current density about 7 μA/cm^2 [11]. After the HPT process on pure magnesium the current density was reported as 8 μA/cm^2 [11]. The current densities for the AZ91 alloy after the first and second passes of the HCEC process were respectively 4.9 and 3.1 μA/cm^2, which are even lower than that of pure magnesium. On the other hand, according to Ref. [10], ECAP processing of the AZ91 alloy has a negative effect on the corrosion current density and increases the current density to the values higher than 140 μA/cm^2, which shows the disability of the ECAP process in corrosion improvement of the AZ91 alloy unlike HCEC. The overall results present a HCEC process as a propriate candidate in improving the corrosion properties of the AZ91 magnesium alloy.

The electrochemical impedance spectrometry measurement like other tests was carried out for the initial AZ91 magnesium alloy and HCEC processed samples and the Nyquist diagrams in the terms of Z'' and Z', which are respectively indicative of the imaginary and the real impedances are presented in Fig. 10(a). All the samples illustrate the capacitive arc. The diameter of the capacitive arc is proportional to metal dissolving in the corrosion environments, which is indicative of corrosion resistance [47]. Moreover, a second arc and tail in the Nyquist diagram is the representative of the inductive characteristic. This arc is proportional to pitting during the corrosion process [48]. However, this type of arc doesn't have any important effect on the investigation of the electrochemical corrosion and subsequently did not investigate in this work [10]. Generally, two trends can be concluded from the Nyquist diagram. Initially, as it is depicted in the diagram, the processed sample shows large diameters, which suggests an improved corrosion resistance after the HCEC process in comparison to the initial condition. Next, by increasing the number of the passes of HCEC process, the diameter of the capacitive arc increases, and subsequently better resistance was achieved. These results are in agreement with the polarization results, showing the improvement in corrosion behavior of the processed sample rather than the initial as-cast one.

Table 3 Comparison of corrosion properties of AZ91 magnesium alloy derived from potentiodynamic tests with other processes for pure magnesium and AZ91magnesium alloy

Process	Material	J_{corr}/(μA·cm^{-2})	φ_{corr}(vs Ag/AgCl)/V	Source
Prior to HCEC (as-cast)	AZ91 Mg	47	−1.46	This study
HCEC-1P	AZ91 Mg	4.9	−1.33	This study
HCEC-2P	AZ91 Mg	3.1	−1.26	This study
Prior to ECAP (as-cast)	AZ91 Mg	19	−1.497	[10]
ECAP-1P	AZ91 Mg	110	−1.495	[10]
ECAP-4P	AZ91 Mg	120	−1.494	[10]
ECAP-8P	AZ91 Mg	130	−1.484	[10]
ECAP-12P	AZ91 Mg	138	−1.476	[10]
Prior to HPT (as-cast)	Pure Mg	7	−1.48	[11]
HPT	Pure Mg	8	−1.49	[11]
Hot roll+ECAP	Pure Mg	40	−1.51	[11]

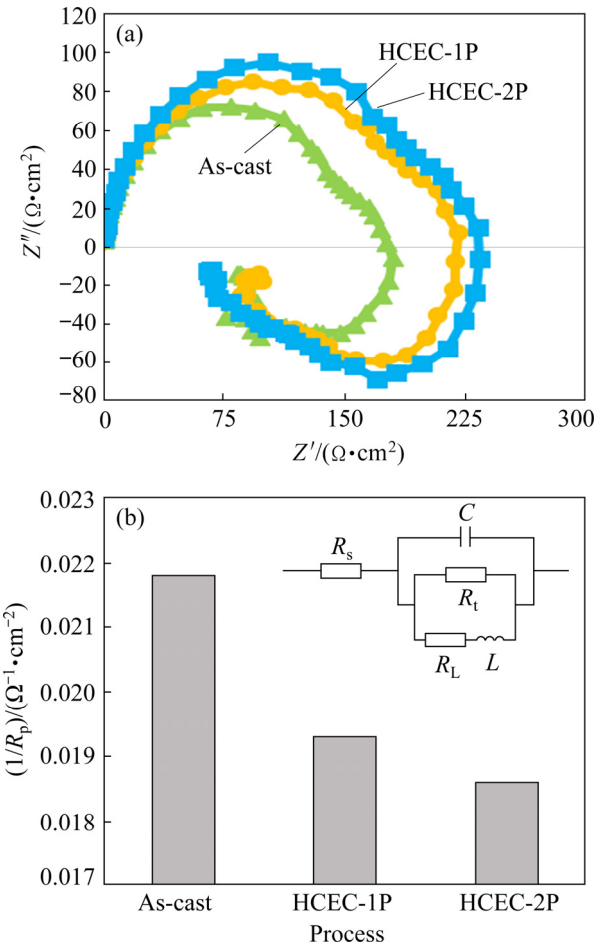

Fig. 10 Nyquist curves for AZ91 magnesium alloy before and after HCEE process (a) and corrosion rate ($1/R_p$) from EIS measurement (b)

To better represent the corrosion resistance by EIS tests, the polarization resistance (R_p), which reciprocal is proportional to the corrosion rate, is calculated and the $1/R_p$ values for the initial sample and processed ones are depicted in Fig. 10(b). To this end, a circuit with an inductive loop was used [49]. The used model is depicted in the corner of Fig. 10(b). In this model, R_s is the resistance of the solution, C represents the double layer capacitance and R_t shows the charge transfer resistance of the magnesium alloy. L and R_L are indicative of the inductance and resistance during the breaking of the fractional protecting layer on the surface [50]. The polarization resistance R_p derived from the EIS test is computed by

$$R_p = R_s + \frac{R_L R_t}{R_L + R_t} \tag{4}$$

As it is depicted in Fig. 10(b), the $1/R_p$ of the sample is decreased by increasing the number of passes, which shows the capability of HCEC in decreasing the corrosion rate of the AZ91 samples.

On the other hand, after fitting the model and deriving the C values, which is related to the electrolyte uptake via the existed defects on the surface of the film, C decreases after the HCEC process. The value of C for the initial sample was 5.36×10^{-6} F/cm. After the second cycle of the process, the C value decreases to 4.5×10^{-6} F/cm. This reduction in C value represents the decrease of the defects in the oxide films [46]. The decrease in C value plays an important role in the reduction of diffusion reaction and subsequently confirmed the improvement in corrosion resistance.

SEM images of the corroded surface after the corrosion measurements in 3.5 wt.% NaCl solution for the unprocessed and processed samples are depicted in Fig. 11. The images confirm the aforementioned variation of corrosion properties after the HCEC process. The corrosion in the initial sample is uniform and whole the surface has the signs of the corrosion. More pits are shown in the initial sample. By performing the HCEC process the corrosion occurred locally in the processed samples and the surface of the two-pass processed samples had a low symptom of the corrosion. Furthermore, there are some regions without any corrosion effects. This shows high resistance of the HCEC processed sample against corrosion and further confirms the ability of the HCEC process in improving the corrosion properties of AZ91 magnesium alloy.

4 Discussion

4.1 Magnesium samples and FEM analysis

Frictional forces have a straight effect on the total force required for forming of the alloys with SPD techniques. On the other hand, the frictional force during the processing of the alloys is directly proportional to the length of the processed sample. By increasing the contact area between the die and sample, the frictional force increases, and subsequently the total forming force increases. This is one of the limiting parameters in disability of the conventional SPD method for producing long samples. One of the ways for decreasing this redundant force is using the fluid between the die and the sample and prevention from direct contact

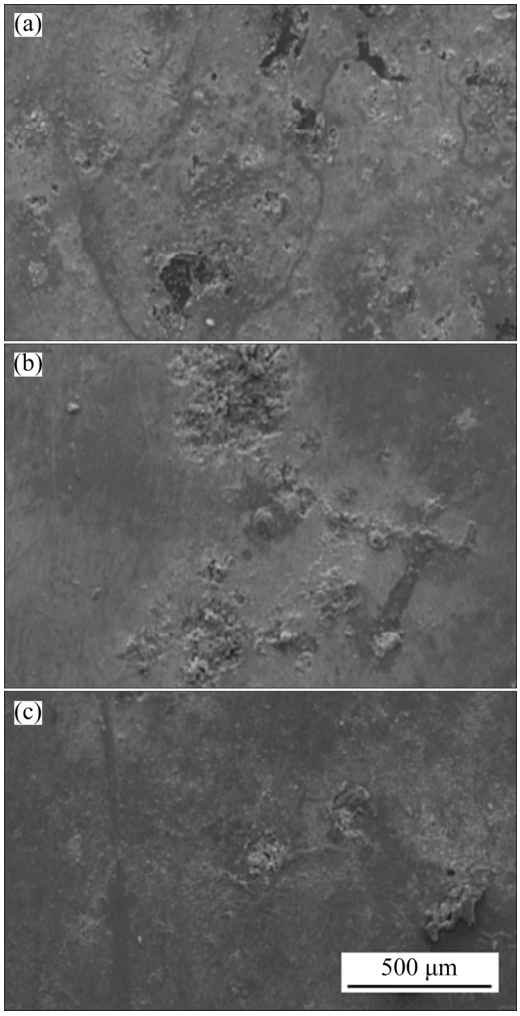

Fig. 11 SEM images of corroded surfaces of unprocessed and HCEC processed AZ91 magnesium rods after corrosion test: (a) Initial sample; (b) One pass; (c) Two passes

of them. However, to process the sample the friction cannot be omitted in the deformation regions. At the same time using the fluid for processing applies high hydrostatic pressure to the sample. This higher hydrostatic pressure is an important element in the processing of alloys and the prevention of crack growth during processing [17]. All of the aforementioned reasons make the HCEC process a notable method to use as a technique for producing ultrafine-grained long samples. Moreover, independency of the process to the length of the sample (Fig. 3) and achieving better strain homogeneity by this process in comparison to the CEC (Fig. 4) are the complementary reasons for using the hydraulic fluid for processing, which has the direct effect in achieving more homogeneous microstructure and better mechanical or corrosion properties [13,15,51]. On the other hand, the buckling of the forming punch is another limiting factor in the conventional process of the long samples. Critical force for buckling of the punch (P_{cr}) is like the simply supported beam, which is calculated from Eq. (5).

$$P_{cr}=\frac{\pi^2 EI}{l^2} \tag{5}$$

where E is the elastic modulus of punch, I is indicative of the second-moment area and l is the length of the punch. In the processing of the materials, usually a steel punch with the elastic modulus of 200 GPa is used. The length of the punch is selected according to the length of the sample. For example, refining the sample with a length of 16 cm (the simulated case in the present study), a punch with the same length is required. By using the punch with a length of 16 cm and a diameter of 12 mm, the P_{cr} of 78.36 kN is obtained. On the other hand, according to the FEM analysis in Fig. 3, the maximum force in the HCEC processing of the magnesium rod with a length of 16 cm is about 49 kN. However, CEC processing of the sample with the same length requires the maximum force of 345 kN, which is 4.4 times the critical force for buckling of punch. This fails the processing punch and makes the CEC processing using the one punch impossible [52]. These are indicative of the worth of the HCEC process in the production of long samples and the necessities for substitution of hydrostatic-based methods with conventional SPD techniques for industrial application.

4.2 Microstructure evaluation

Conducting the HCEC process on AZ91 magnesium alloy leads to the major decrease in the size of the grains and combination of the ultrafine-grained grains regions with partially unrecrystallized zone and undissolved $Mg_{17}Al_{12}$ the structure was obtained after the process. Schematic representation of the grain refinement of AZ91 magnesium alloy during HCEC is depicted in Fig. 12. There are some factors, which are responsible for grain refinement of the alloy after the process. The most important factors are high strain, temperature, twinning, and dynamic recrystallization [44]. A high shear strain is applied to sample at a high temperature, which leads to the

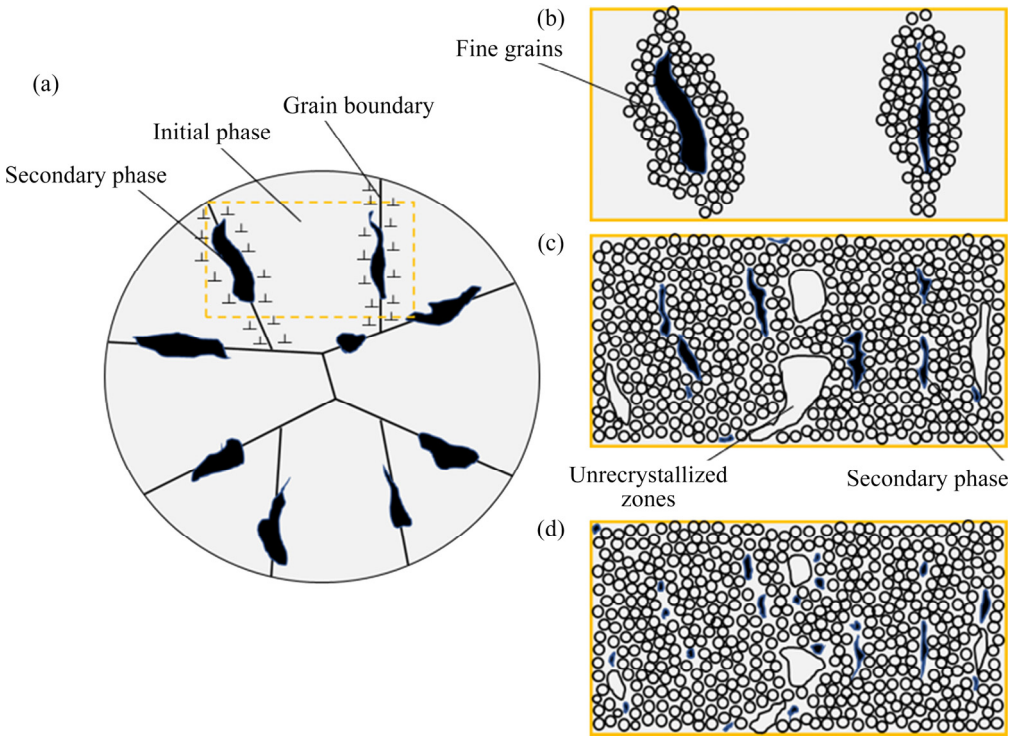

Fig. 12 Schematic representation of grain refinement of AZ91 magnesium alloy during HCEC: (a) Initial state; (b) During deformation; (c) After the first cycle; (d) After the second cycle

variation in dislocation density, twinning in original grains and also the occurrence of the dynamic recrystallization in the sample, and the formation of the fine grains within the initial grains. The occurrence of dynamic recrystallization was also reported in different studies as an agent for grain refinement in the SPD processing of magnesium alloy at elevated temperature [44,53,54]. Furthermore, $Mg_{17}Al_{12}$ is another important factor in the formation of fine-grained microstructure after the SPD techniques. By imposing a higher strain at a higher temperature $Mg_{17}Al_{12}$ particles are broken in small parts. Their effect in microstructure is mainly dependent on their size. Finer particles can act as an obstacle for the growth of the recrystallized grains. In contrast, coarse ones can speed up the recrystallization through the particle stimulating nucleation (PSN) mechanism [55−57]. As depicted in Fig. 12(c) after the first cycle more elongated and large $Mg_{17}Al_{12}$ particles exist, which makes the PSN as the major mechanism after the first cycle. However, at the same time, fine particles are available, which plays the role of the pinning effect. The newly nucleated grain at grain boundaries and along the impurities started to grow. During their growth, they reach the fine particles. On the other hand, magnesium is a material with low stacking fault energy. Most of the boundaries of nucleated grain cannot pass through the particles and their growth is restricted and subsequently, the fine-grained microstructure is achieved. By performing the second pass, most of the particles are crushed to small ones and as presented in Fig. 12(d), combination of the finer $Mg_{17}Al_{12}$ particles and dynamic recrystallization leads to the more homogenous microstructure.

4.3 Microhardness and tensile strength

There are two main parameters which have a direct effect on the mechanical properties of the processed alloys by SPD techniques. The first parameter is grain size. According to the Hall−Petch relationship, the strength of the alloys increases by decreasing the grain size [58]. The reduction in grain size is shown in Fig. 5 after processing the AZ91 magnesium alloy by the HCEC process. The second parameter is the existence of the second phase and its distribution [3]. During the casting of the AZ91 magnesium alloys, a high amount of β phases form at grain boundaries. This hard particle has an opposing effect on the mechanical characteristic of

the alloy and can act as an agent for reducing the elongation, which is obvious in the stress−strain curve of the as-cast alloy in Fig. 7(a) [44]. Another important reason in lower mechanical properties of the AZ91 alloy is the existence of lower slip systems in magnesium alloy [59]. Performing the SPD processes usually refines the microstructure of the alloys and subsequently leads to an increase in strength. Furthermore, breaking the second phase particle is another factor in increasing the strength and also elongation in magnesium alloys after the SPD techniques [40]. These procedures are done like other SPD techniques in the AZ91 magnesium alloy after the HCEC process. But there are some important factors in the HCEC process, which distinguish it from the other techniques and as depicted in Fig. 7(b) leads to outstanding properties than other processes. These factors are using high hydrostatic compressive pressure along with high shear strains for forming. The hydrostatic pressure is useful in eliminating the onset of the cracks and its distribution during the process. Also, it helps in applying more homogenous strain to sample than conventional methods, which is depicted in Fig. 4 in FEM analysis. Additionally, it is responsible in achieving ultrafine grains with higher angle of grain boundaries [60]. All of these factors are the reasons for obtaining the more superior mechanical properties with the HCEC process. Performing the second pass of the HCEC process causes better distributing of the intermetallic phase and more reduction in grain size and forming of the equiaxed grains [41,61]. These can count as the factors for improving the mechanical properties and especially ductility after the second cycle of HCEC.

Microhardness values also have an intense dependency on grain refinement according to the Hall−Petch relationship for hardness [17]. Furthermore, the hardness of the second phase in AZ91 magnesium alloy is considerably higher in comparison to the α-phase [37]. So, the increase of the microhardness after the HCEC process can be attributed to the homogeneous distribution of β-phase after the process along with the decrease in grain size. The fluctuation in hardness is in accordance with the amount of the second phase and also the existence of some unrecrystallized zones in the cross-section. Also, other parameters such as dislocation, strain hardening, and texture are effective [62]. Moreover, the higher strain and better homogeneity in its distribution after the second cycle of the process returns to the more uniform microstructure and distribution of the strain, which was depicted by strain homogeneity index calculated by FEM analysis. The better hardness of the HCEC processed sample in comparison to other SPD techniques is again due to the effects of the higher hydrostatic pressure by the HCEC process.

4.4 Corrosion behavior evaluation

According to the polarization and EIS measurement in Figs. 9 and 10, better corrosion resistance is shown after the HCEC processing of the AZ91 magnesium alloy. This improvement in corrosion behavior became more by increasing the number of passes of the HCEC process to the second cycle. The enhancement in corrosion properties is in accordance with some studies such as CEC processing of the Mg−Nd−Zn−Zr alloy or HPT processing of the pure magnesium [11,63]. However, it is in contradiction with other studies such as ECAP processing of AZ91 alloy [10]. These variations in trends after the SPD techniques can attribute to the application of the higher compressive force during processes such as CEC and HPT. This higher compressive force is accompanied by more homogeneous strain in the HCEC process, which leads to superior corrosion properties in comparison to other SPD techniques. Generally, there are some events, which occur during the processing of the AZ91 magnesium alloy by HCEC and improves the corrosion resistance. The first important event is refining the grains to the ultrafine scales. Grain refinement can act as an agent for preventing the rupture in the formed hydroxide layer on the surface by relieving the compressive force, which was formed during the conversion of unstable oxide layer to magnesium hydroxide in the aqueous solution due to hydration. Also, grain refinement leads to the formation of some isolated magnesium oxide nanocrystals between the oxide layer and base alloy and restricts the stress gradient and subsequently decreases the corrosion rate [64]. Furthermore, the effects of grain refinement in reducing the crystallographic pitting propagation (PCP) were reported as a factor in the reduction of the corrosion rate in some studies [65]. Also, it was reported that compressive residual stresses, which formed during the processing in materials have positive effects in

improving the corrosion behavior [66]. HCEC method is among the processes, which applies a higher compressive force to the samples, and subsequently, this is one of the reasons for better performance of the HCEC processed sample with increasing the number of cycles. On the other hand, the second phase can count as the other effective parameters in the corrosion properties of the AZ91 magnesium alloys. As it is depicted in the micrographs of the HCEC processed rod, the second phase particles were broken into small parts after processing and their distribution and size become more uniform after the second cycle, which is an important factor in reducing the galvanic corrosion [63,67]. So, the combination of these variations by HCEC leads to the low corrosion rate in HCEC processed sample, which is depicted clearly in the SEM images of the corroded surface after EIS measurement in Fig. 11.

5 Conclusions

(1) HCEC process provided a special combination of the characteristics such as the production of the samples with a high length to diameter ratio, application of high hydrostatic compressive force, and more homogenous strain to the sample, which has not been shown by other SPD techniques.

(2) The forming forces of the HCEC process of the sample with the lengths of 8 and 16 cm were almost the same. However, processing identical samples without the usage of hydraulic fluid gave different results. The forming force for processing the longer sample was 3.2 times that of the shorter one.

(3) OM and SEM images illustrated the capability of the HCEC process in grain refinement of the AZ91 magnesium rods. The different microstructure in comparison to the initial sample with mostly refined grains in the range of 1−3 μm was achieved.

(4) The increase in ultimate strength after the first cycle and second cycles were 1.94 and 2.46 times the initial values, respectively. Also, the elongation increased to 8% and 14% after the first and second cycles in comparison to the initial value of 3.8%.

(5) The microhardness values were increased as like as the strength. The average microhardness values were HV 99.1 and HV 107.6 comparing the initial value of HV 49.8.

(6) Polarization curves indicated the outstanding improvement of the HCEC processed sample. The currents were lower after the process and the obtained polarization resistances after the first and second cycles of the HCEC process were 3.5 and 5 times that of the initial sample.

(7) The Nyquist diagrams showed greater capacitive arcs for the HCEC processed samples and the obtained corrosion rate showed the improvement in corrosion behavior for the processed samples.

(8) The SEM micrographs of the corroded surfaces showed a decrease in corrosion rate and change of the uniform overall corrosion in the unprocessed sample to local corrosion in the HCEC processed samples.

Acknowledgments

This work was supported by Iran National Science Foundation (INSF).

References

[1] KULEKCI M K. Magnesium and its alloys applications in automotive industry [J]. The International Journal of Advanced Manufacturing Technology, 2008, 39: 851−856.

[2] MUELLER W D, NASCIMENTO M L, de MELE M F L. Critical discussion of the results from different corrosion studies of Mg and Mg alloys for biomaterial applications [J]. Acta Biomaterialia, 2010, 6: 1749−1755.

[3] DING Han-lin, LIU Liu-fa, KAMADO S, DING Wen-jiang, KOJIMA Y. Study of the microstructure, texture and tensile properties of as-extruded AZ91 magnesium alloy [J]. Journal of Alloys and Compounds, 2008, 456: 400−406.

[4] TANG Chao-lan, LI Hao, LI Sai-yi. Effect of processing route on grain refinement in pure copper processed by equal channel angular extrusion [J]. Transactions of Nonferrous Metals Society of China, 2016, 26: 1736−1744.

[5] SAMADPOUR F, FARAJI G, SIAHSARANI A. Processing of AM60 magnesium alloy by hydrostatic cyclic expansion extrusion at elevated temperature as a new SPD method [J]. International Journal of Minerals, Metallurgy and Materials, 2020, 27: 669−677.

[6] LI Ping, XUE Ke-min, WANG Xiao-xi, QIAN Chen-hao. Refinement and consolidation of pure Al particles by equal channel angular pressing and torsion [J]. Transactions of Nonferrous Metals Society of China, 2014, 24: 1289−1294.

[7] WANG Li-ping, CHEN Tian, JIANG Wen-yong, FENG Yi-cheng, CAO Guo-jian, ZHU Yan. Microstructure and mechanical properties of AM60B magnesium alloy prepared by cyclic extrusion compression [J]. Transactions of nonferrous metals society of China, 2013, 23: 3200−3205.

[8] ZHILYAEV A P, LANGDON T G. Using high-pressure torsion for metal processing: Fundamentals and applications [J]. Progress in Materials Science, 2008, 53: 893−979.

[9] RAHMATABADI D, TAYYEBI M, HASHEMI R, FARAGI G. Microstructure and mechanical properties of Al/Cu/Mg laminated composite sheets produced by the ARB process [J]. International Journal of Minerals, Metallurgy, and Materials, 2018, 25: 564−572.

[10] SONG Dan, MA Ai-bin, JIANG Jing-hua, LIN Ping-hua, YANG Dong-hui, FAN Jun-feng. Corrosion behaviour of bulk ultra-fine grained AZ91D magnesium alloy fabricated by equal-channel angular pressing [J]. Corrosion Science, 2011, 53: 362−373.

[11] SILVA C, OLIVIERA A C, COSTA C, FIGUEIREDO R, FATIMA LEITE M, PEREIRA M, LINS V, LANGDON T. Effect of severe plastic deformation on the biocompatibility and corrosion rate of pure magnesium [J]. Journal of Materials Science, 2017, 52: 5992−6003.

[12] WU Qiong, ZHU Shi-jie, WANG Li-guo, LIU Qian, YUE Gao-chao, WANG Jun, GUAN Shao-kang. The microstructure and properties of cyclic extrusion compression treated Mg−Zn−Y−Nd alloy for vascular stent application [J]. Journal of the Mechanical Behavior of Biomedical Materials, 2012, 8: 1−7.

[13] SAMADPOUR F, FARAJI G, BABAIE P, BEWSHER S, MOHAMMADPOUR M. Hydrostatic cyclic expansion extrusion (HCEE) as a novel severe plastic deformation process for producing long nanostructured metals[J]. Materials Science and Engineering A, 2018, 718: 412−417.

[14] SIAHSARANI A, SAMADPOUR F, MORTAZAVI M, FARAJI G. Microstructural, mechanical and corrosion properties of AZ91 magnesium alloy processed by a severe plastic deformation method of hydrostatic cyclic expansion extrusion [J]. Metals and Materials International, 2020, DOI: 10.1007/s12540-020-00828-0.

[15] JAMALI S, FARAJI G, ABRINIA K. Hydrostatic radial forward tube extrusion as a new plastic deformation method for producing seamless tubes [J]. The International Journal of Advanced Manufacturing Technology, 2017, 88: 291−301.

[16] PACHLA W, KULCZYK M, SUS-RYSZKOWSKA M, MAZUR A, KURZYDLOWSKI K. Nanocrystalline titanium produced by hydrostatic extrusion [J]. Journal of Materials Processing Technology, 2008, 205: 173−182.

[17] FARAJI G, KIM H. S, KASHI H. T. Severe plastic deformation: Methods, processing and properties [M]. Amsterdam: Elsevier, 2018.

[18] SIAHSARANI A, FARAJI G. Hydrostatic cyclic extrusion compression (HCEC) process: A new CEC counterpart for processing long ultrafine-grained metals [J]. Archives of Civil and Mechanical Engineering, 2020, 20: 1−13.

[19] RICHERT M W. Features of cyclic extrusion compression: Method, structure & materials properties [J]. Solid State Phenomena, 2006, 114: 19−28.

[20] STEPANEK R, PANTELEJEV L, MAN O. Thermal stability of magnesium alloy AZ91 prepared by severe plastic deformation [J]. Materials Engineering, 2016, 20: 160−166.

[21] RHEE K, HAN W Y, PARK H J, KIM S S. Fabrication of aluminum/copper clad composite using hot hydrostatic extrusion process and its material characteristics [J]. Materials Science and Engineering A, 2004, 384: 70−76.

[22] SU C W, LU L, LAI M O. 3D finite element analysis on strain uniformity during ECAP process [J]. Materials Science and Technology, 2007, 23: 727−735.

[23] YAMASHITA A, HORITA Z, LANGDON T. Improving the mechanical properties of magnesium and a magnesium alloy through severe plastic deformation [J]. Materials Science and Engineering A, 2001, 300: 142−147.

[24] TOFIL A, PATER Z. Overview of the research on roll forging processes [J]. Advances in Science and Technology-Research Journal, 2017: 11: 72−86.

[25] ZHANG Lu-jun, WANG Qu-dong, CHEN Yong-jun, LIN Jin-bao. Microstructure evolution and mechanical properties of an AZ61 Mg alloy through cyclic extrusion compression [J]. Materials Science Forum, 2007, 546: 253−256.

[26] RICHERT M, RICHERT J, ZASASZINSKI J, HAWRYLKIEWICZ S, DLUGOPOLSKI J. Effect of large deformations on the microstructure of aluminium alloys [J]. Materials Chemistry and Physics, 2003, 81: 528−530.

[27] RICHERT M, STUWE H, ZEHETBAUER H, RICHERT J, PIPPAN R, MOTZ C, SCHAFLER E. Work hardening and microstructure of AlMg5 after severe plastic deformation by cyclic extrusion and compression [J]. Materials Science and Engineering A, 2003, 355: 180−185.

[28] KARAMIŞ M B, SARI N F, ERTURUN V. Friction and wear behaviors of reciprocatingly extruded Al−SiC composite [J]. Journal of Materials Processing Technology, 2012, 212: 2578−2585.

[29] RICHERT M, LIU Qing, HANSEN M. Microstructural evolution over a large strain range in aluminium deformed by cyclic-extrusion–compression [J]. Materials Science and Engineering A, 1999, 260: 275−283.

[30] RICHERT M, MCQUEEN H, RICHERT J. Micrbband formation in cyclic extrusion compression of aluminum [J]. Canadian Metallurgical Quarterly, 1998, 37: 449−457.

[31] ZHANG Li, WANG Qu-dong, LIAO Wen-jun, GUO Wei, LI Wen-zhen, JIANG Hai-yan, DING Wen-jiang. Microstructure and mechanical properties of the carbon nanotubes reinforced AZ91D magnesium matrix composites processed by cyclic extrusion and compression [J]. Materials Science and Engineering A, 2017, 689: 427−434.

[32] HUANG Hua, TANG Zibo, TIAN Yuan, JIA Gao-zhi, NIU Jia-lin, ZHANG Hua, PEI Jia, YUAN Guang-yin, DING Wen-jiang. Effects of cyclic extrusion and compression parameters on microstructure and mechanical properties of Mg−1.50Zn−0.25 Gd alloy [J]. Materials & Design, 2015, 86: 788−796.

[33] LIN Jin-bao, WANG Xin-yi, REN Wei-jie, YANG Xue-xia, WANG Qu-dong. Enhanced strength and ductility due to microstructure refinement and texture weakening of the GW102K alloy by cyclic extrusion compression [J]. Journal of Materials Science & Technology, 2016, 32: 783−789.

[34] AMANI S, FARAJI G, ABRINIA K. Microstructure and hardness inhomogeneity of fine-grained AM60 magnesium alloy subjected to cyclic expansion extrusion (CEE) [J]. Journal of Manufacturing Processes, 2017, 28: 197−208.

[35] SAMADPOUR F, SIAHSARANI A, FARAJI G, BAHRAMI M. Experimental and finite element analyses of the hydrostatic cyclic expansion extrusion (HCEE) process with

back-pressure [J]. Journal of Ultrafine Grained and Nanostructured Materials, 2019, 52: 25−31.

[36] WANG Lei, ZHANG Bo-Ping, SHINIHARA T. Corrosion behavior of AZ91 magnesium alloy in dilute NaCl solutions [J]. Materials & Design, 2010, 31: 857−863.

[37] FARAJI G, YAVARI P, AGHDAMIFAR M, MASHHADI M M. Mechanical and microstructural properties of ultra-fine grained AZ91 magnesium alloy tubes processed via multi pass tubular channel angular pressing (TCAP) [J]. Journal of Materials Science & Technology, 2014, 30: 134−138.

[38] MATHIS K, GUBICZA J, NAM N H. Microstructure and mechanical behavior of AZ91 Mg alloy processed by equal channel angular pressing [J]. Journal of Alloys and Compounds, 2005, 394: 194−199.

[39] TAN Ming, LIU Zhao-ming, QUAN Gao-feng. Effects of hot extrusion and heat treatment on mechanical properties and microstructures of AZ91 magnesium alloy [J]. Energy Procedia, 2012, 16: 457−460.

[40] ENSAFI M, FARAJI G, ABDOLVAND H. Cyclic extrusion compression angular pressing (CECAP) as a novel severe plastic deformation method for producing bulk ultrafine grained metals [J]. Materials Letters, 2017, 197: 12−16.

[41] FATA A, FARAJI G, MASHHADI M M, TAVAKKOLI V. Hot deformation behavior of Mg−Zn−Al alloy tube processed by severe plastic deformation [J]. Archives of Metallurgy and Materials, 2017, 62: 159−166.

[42] ZHANG Xiao-hua, CHENG Yuan-sheng. Tensile anisotropy of AZ91 magnesium alloy by equal channel angular processing [J]. Journal of Alloys and Compounds, 2015, 622: 1105−1109.

[43] JAMALI S, FARAJI G, ABRINIA K. Evaluation of mechanical and metallurgical properties of AZ91 seamless tubes produced by radial-forward extrusion method [J]. Materials Science and Engineering A, 2016, 666: 176−183.

[44] FATA A, FARAJI G, MASHHADI M M, ABDOLVAND H. Evaluation of hot tensile behavior of fine-grained Mg−9Al−1Zn alloy tube processed by severe plastic deformation [J]. Transactions of the Indian Institute of Metals, 2017, 70: 1369−1376.

[45] BORKO K, FINTOVA S, HADZIMA B. Linear potentiodynamic characterization of ECAPed biocompatible AZ91 magnesium alloy [J]. Materials Science Forum, 2017, 891: 404−408.

[46] SINGH I, SINGH M, DAS S. A comparative corrosion behavior of Mg, AZ31 and AZ91 alloys in 3.5% NaCl solution [J]. Journal of Magnesium and Alloys, 2015, 3: 142−148.

[47] CAO Chu-nan. On the impedance plane displays for irreversible electrode reactions based on the stability conditions of the steady-state—I: One state variable besides electrode potential [J]. Electrochimica Acta, 1990, 35: 831−836.

[48] METIKOS-HUKOVIĆ M, BABIC R, GRUBAC Z, BRINC S. Impedance spectroscopic study of aluminium and Al-alloys in acid solution: Inhibitory action of nitrogen containing compounds [J]. Journal of Applied Electrochemistry, 1994, 24: 772−778.

[49] ZHANG Tao, SHAO Ya-wei, MENG Guo-zhe, CUI Zhong-yu, WANG Fu-hui. Corrosion of hot extrusion AZ91 magnesium alloy: I-Relation between the microstructure and corrosion behavior [J]. Corrosion Science, 2011, 53: 1960−1968.

[50] AUNG N N, ZHOU Wei. Effect of grain size and twins on corrosion behaviour of AZ31B magnesium alloy [J]. Corrosion Science, 2010, 52: 589−594.

[51] SAVARABADI M M, FARAJI G, EFTEKHARI M. Microstructure and mechanical properties of the commercially pure copper tube after processing by hydrostatic tube cyclic expansion extrusion (HTCEE) [J]. Metals and Materials International. https://doi.org/10.1007/s12540-019-00525-7.

[52] ARTAN R, TEPE A. The initial values method for buckling of nonlocal bars with application in nanotechnology [J]. European Journal of Mechanics-A/Solids, 2008, 27: 469−477.

[53] ZHANG Ding-fei, HU Hong-jun, PAN Fu-sheng, YANG Ming-bo, ZHANG Jun-ping. Numerical and physical simulation of new SPD method combining extrusion and equal channel angular pressing for AZ31 magnesium alloy [J]. Transactions of Nonferrous Metals Society of China, 2010, 20: 478−483.

[54] FATEMI M, ZAREI-HANZAKI A, CABRERA J M, CALVILLO P R. EBSD characterization of repetitive grain refinement in AZ31 magnesium alloy [J]. Materials Chemistry and Physics, 2015, 149: 339−343.

[55] SCHAFER C, SONG J, GOTTSTEIN G. Modeling of texture evolution in the deformation zone of second-phase particles [J]. Acta Materialia, 2009, 57: 1026−1034.

[56] ROBSON J, HENRY D, DAVIS B. Particle effects on recrystallization in magnesium–manganese alloys: Particle-stimulated nucleation [J]. Acta Materialia, 2009, 57: 2739−2747.

[57] TROEGER L P, STARKE E A. Particle-stimulated nucleation of recrystallization for grain-size control and superplasticity in an Al−Mg−Si−Cu alloy [J]. Materials Science and Engineering A, 2000, 293: 19−29.

[58] YUAN Wei, PANIGRAHI S, SU Jian-qing, MISHRA R. Influence of grain size and texture on Hall–Petch relationship for a magnesium alloy [J]. Scripta Materialia, 2011, 65: 994−997.

[59] CHINO Y, KOBATA M, IWASAKI H, MABUCHI M. An investigation of compressive deformation behaviour for AZ91 Mg alloy containing a small volume of liquid [J]. Acta Materialia, 2003, 51: 3309−3318.

[60] KRAWCZYNSKA A T, GIERLOTKA S, SUCHECKI P, SETMAN D, ADAMCZYK-CIESLAK B, LEWANDOWSKA M, ZEHETBAUER M. Recrystallization and grain growth of a nano/ultrafine structured austenitic stainless steel during annealing under high hydrostatic pressure [J]. Journal of Materials Science, 2018, 53: 11823−11836.

[61] MASOUDPANAH S M, MAHMUDI R. The microstructure, tensile, and shear deformation behavior of an AZ31 magnesium alloy after extrusion and equal channel angular pressing [J]. Materials & Design, 2010, 31: 3512−3517.

[62] FARAJI G, MASHHADI M M, KIM H S. Tubular channel angular pressing (TCAP) as a novel severe plastic deformation method for cylindrical tubes [J]. Materials

Letters, 2010, 65: 3009−3012.
[63] ZHANG Xiao-bo, YUAN Guang-yin, WANG Zhang-zhong. Mechanical properties and biocorrosion resistance of Mg−Nd−Zn−Zr alloy improved by cyclic extrusion and compression [J]. Materials Letters, 2012, 74: 128−131.
[64] AHMADKHANIHA D, FEDEL M, SOHI M H, DEFLORIAN F. Corrosion behavior of severely plastic deformed magnesium based alloys: A review [J]. Surface Engineering and Applied Electrochemistry, 2017, 53: 439−448.
[65] HAN G, LEE J Y, KIM Y C, PARK J H, KIM D I, HAN H S, YANG S J, SEOK H K. Preferred crystallographic pitting corrosion of pure magnesium in Hanks' solution [J]. Corrosion Science, 2012, 63: 316−322.
[66] SEONG J W, KIM W J. Development of biodegradable Mg−Ca alloy sheets with enhanced strength and corrosion properties through the refinement and uniform dispersion of the Mg2Ca phase by high-ratio differential speed rolling [J]. Acta Biomaterialia, 2015, 11: 531−542.
[67] PENG Qiu-ming, LI Xue-jun, MA Ning, LIU Ri-ping, ZHANG Hong-jie. Effects of backward extrusion on mechanical and degradation properties of Mg–Zn biomaterial [J]. Journal of the Mechanical Behavior of Biomedical Materials, 2012, 10: 128−137.

新型强塑性变形—静液循环挤压压缩加工 AZ91 镁合金及其表征

Armin SIAHSARANI, Ghader FARAJI

School of Mechanical Engineering, College of Engineering, University of Tehran, Tehran, 11155-4563, Iran

摘　要：通过静液循环挤压压缩(HCEC)强塑性变形法加工具有较大高径比的密排六方金属棒，并研究其性能。对 AZ91 镁合金进行两个连续循环加工，研究其显微组织演化、力学性能和腐蚀行为。结果表明，HCEC 加工可成功制备超细晶镁合金长棒材，且可同时提高其强度和韧性。经二次循环加工后，样品的抗拉强度和伸长率分别为铸态样品的 2.46 倍和 3.8 倍，显微硬度分布更加均匀，其平均值增加了 116%。对于加工后的样品，从极化曲线得到的电位较高，电流较低，从 Nyquist 曲线得到的电容弧直径更大。有限元分析表明，与传统的循环挤压压缩相比，HCEC 载荷与长度无关。HCEC 是一种特殊的强塑性变形方法，可以制备兼具良好力学性能和耐腐蚀性能的超细晶镁合金长棒材。

关键词：强塑性变形；循环挤压压缩；腐蚀行为；力学性能；静液压力

(Edited by Xiang-qun LI)